SCIENCE CHINA
Earth Sciences

• RESEARCH PAPER •

November 2012 Vol.55 No.11: 1919–1928
doi: 10.1007/s11430-012-4454-8

Extraction of line-of-sight ionospheric observables from GPS data using precise point positioning

ZHANG BaoCheng[1,2*], OU JiKun[1], YUAN YunBin[1] & LI ZiShen[1,2]

[1] *State Key Laboratory of Geodesy and Earth's Dynamics, Institute of Geodesy and Geophysics, Chinese Academy of Sciences, Wuhan 430077, China;*
[2] *Graduate University of Chinese Academy of Sciences, Beijing 100049, China*

Received February 13, 2011; accepted March 26, 2012; published online July 18, 2012

Here we propose a method for extracting line-of-sight ionospheric observables from GPS data using precise point positioning (PPP). The PPP-derived ionospheric observables (PIOs) have identical form with their counterparts obtained from leveling the geometry-free GPS carrier-phase to code (leveling ionospheric observables, LIOs), and are affected by the satellite and receiver inter-frequency biases (IFBs). Based on the co-location experiments, the effects of extracting error arising from the observational noise and multipath on the PIOs and the LIOs are comparatively assessed, and the considerably reduced effects ranging from 70% to 75% on the PIOs with respect to the LIOs can be verified in our case. In addition, based on 26 consecutive days' GPS observations from two international GNSS service (IGS) sites (COCO, DAEJ) during disturbed ionosphere period, the extracted PIOs and LIOs are respectively used as the input of single-layer ionospheric model to retrieve daily satellite IFBs station-by-station. The minor extracting errors underlying the PIOs in contrast to the LIOs can also be proven by reducing day-to-day scatter and improving between-receiver consistency in the retrieved satellite IFBs values.

line-of-sight ionospheric observables, total electron content (TEC), precise point positioning (PPP), inter-frequency bias (IFB), extracting error

Citation: Zhang B C, Ou J K, Yuan Y B, et al. Extraction of line-of-sight ionospheric observables from GPS data using precise point positioning. Sci China Earth Sci, 2012, 55: 1919–1928, doi: 10.1007/s11430-012-4454-8

In the last decade, the Global Positioning System (GPS) has become a cost-effective and powerful tool for geodesy and geophysics [1–4], especially for calibration of ionospheric total electron content (TEC) along a trajectory, usually, the vertical from the Earth's surface to a specified height in the ionosphere (namely, vertical or vTEC) [5, 6] or ray path from GPS satellite to receiver (slant or sTEC) [7, 8]. The prerequisite for calibrating the GPS-based TEC is the extraction of high-precision ionospheric observables (also called ionospheric measurements or TEC measurements, see [9, 10]) related to the sTEC along the satellite-receiver line-of-sight from dual frequency GPS observations [11, 12]. According to the literatures devoted to GPS-based ionosphere studies, the routinely used ionospheric observables can be categorized as follows:

Code ionospheric observables (CIOs), which can be derived from differencing dual frequency GPS code observations, are modeled as the sum of sTEC, receiver and satellite inter-frequency biases (IFBs) [13, 14]. Due to severe contamination of multipath effects [15], CIOs can only be used for removing the ambiguities from the carrier-phase ionospheric observables (known as "carrier-to-code leveling process", as detailed below).

Carrier-phase ionospheric observables (CPIOs), quite similar to CIOs, can result from subtraction of simultaneous dual frequency GPS carrier-phase observations, in which only the ionospheric and any other frequency-dependent

*Corresponding author (email: b.zhang@whigg.ac.cn)

effects remain. The effects of multipath on CPIOs can be expected to be 100× smaller than the ones on CIOs [7, 13]. However, calibration of sTEC with CPIOs involves estimation of approximately three times more calibration biases than with CIOs [7], because the satellite-dependent IFBs underlying the CIOs are replaced by the arc-dependent ambiguities in CPIOs.

By comparatively analyzing CIOs and CPIOs, two major issues can be addressed: (1) CIOs can provide an absolute measure of sTEC but are prone to severe effects of noise and multipath from code observations [15]; and (2) the CPIOs can provide very precise measurements of TEC changes and free from the aforementioned errors induced by code observations, but at the price of introducing three times more calibration biases than the CIOs [7]. Fortunately, by combining the CIOs and CPIOs with the so-called "carrier-to-code leveling process", the leveling ionospheric observables (LIOs) that are the synthesis of the positive characteristics of both CIOs and CPIOS can be obtained [16, 17].

In addition, double-differenced ionospheric observables (DIOs) can be obtained from double differencing the CPIOs and fixing the double-differenced carrier-phase ambiguities to correct integer values [18, 19]. Studying ionosphere with DIOs is simplified because satellite and receiver specific biases cancel out to the greatest extent. Typical application of DIOs for modeling ionosphere is the prevalent Network-based Real-Time Kinematic (NRTK) technique [20]. However, ionosphere study with DIOs is impossible using single GPS receiver; at the same time, the double-differencing procedure can reduce the ionospheric signal considerably [19].

To date, the LIOs can be deemed as the most suitable ionospheric observables for GPS-related ionosphere studies [5, 6, 9, 11]. According to references [8] and [13], the ultimate accuracy of sTEC estimation based on LIOs can be affected by two systematic errors, namely the extracting error underlying the LIOs, mainly due to the translation of multipath in the CIOs to the LIOs and the model error caused by misspecification of the ionospheric model that have been used for separating sTEC and IFBs. The extracting error is receiver/antenna-dependent, whose multipath component can exceed several TECu; whereas the model error evaluated from synthetic data (free from extracting error) using single-layer ionosphere model can be considered to be in the order of several to several tens of TECu during the period of calm or disturbed ionosphere activities.

Largely reduced model error can be observed if the following two conditions are imposed upon during sTEC estimation: (1) ionospheric observables extracted from multiple receivers' GPS observations are combined (known as multi-site technique, see ref. [21]), and (2) several well-performed ionospheric models, e.g. tomography [22], multi-layer, etc., for ionosphere representation are dedicatedly chosen. But, as the extracting error of LIOs is much more related to the environments around the receiver/antenna than the model error, its attenuating effects on estimated sTEC cannot be relied on combing LIOs from multiple receivers or using practiced ionosphere modeling approaches as experienced by model error.

In this paper, a method for extraction of ionospheric observables with precise point positioning (PPP) technique is presented. The PPP-derived ionospheric observables (PIOs) have coincidently the identical form as the LIOs but are less affected by the extracting error. The discrepancy of extracting ionospheric observables with PPP or with "carrier-to-code leveling process" in essence lies in the procedure chosen to reduce the carrier-phase ambiguities from CPIOs: PPP estimates the ambiguities by performing a geodetic data processing and then reducing their effects from the CPIOs, whereas with carrier-to-code leveling procedure such ambiguities are computed by (weighted) averaging the difference between CIOs and CPIOs for every continuous arc.

1 Extraction of ionospheric observables

1.1 Carrier-to-code leveling process

The dual-frequency GPS code and carrier-phase observation equations in units of length are given below for a receiver-satellite combination $r-s$:

$$\begin{aligned} p^s_{r,j}(i) &= \rho^s_r(i) + \mu_j \cdot I^s_{r,1}(i) - b^s_{,j} + b_{r,j} + \varepsilon_p(i), \\ \phi^s_{r,j}(i) &= \rho^s_r(i) - \mu_j \cdot I^s_{r,1}(i) + N^s_{r,j} + \varepsilon_\phi(i), \end{aligned} \tag{1}$$

where $p^s_{r,j}(i)$ and $\phi^s_{r,j}(i)$ are the GPS code and carrier-phase observations; j and i refer to frequency and epoch indices; $\rho^s_r(i)$ is the lumping frequency-independent effects on GPS signal; $I^s_{r,1}(i)$ is the ionospheric group delay on the first frequency, and the scalar $\mu_j = f_1^2 / f_j^2$ is used to convert such delay to other frequencies; $b^s_{,j}$ and $b_{r,j}$ are the satellite and receiver code biases; $N^s_{r,j}$ is the carrier-phase ambiguity (in length) lumped with phase biases; $\varepsilon_p(i)$ and $\varepsilon_\phi(i)$ refer to the combinations of observational noise and multipath (un-modeled errors) in code and carrier-phase observations.

Hence, by subtracting two carrier-phase, $\phi^s_{r,1}(i)$ and $\phi^s_{r,2}(i)$, and two code observations, $p^s_{r,2}(i)$ and $p^s_{r,1}(i)$, the CPIOs and CIOs in units of TECu can be respectively obtained:

$$\begin{aligned} L^s_{r,I}(i) &= \kappa\left(\phi^s_{r,1}(i) - \phi^s_{r,2}(i)\right) = I^s_{r,t}(i) + \kappa\left(N^s_{r,1} - N^s_{r,2}\right) + \varepsilon_L(i), \\ P^s_{r,I}(i) &= \kappa\left(p^s_{r,2}(i) - p^s_{r,1}(i)\right) = I^s_{r,t}(i) + \kappa\left(b_r - b^s\right) + \varepsilon_P(i), \end{aligned} \tag{2}$$

where $1/\kappa = 40.28\left(\frac{1}{f_2^2} - \frac{1}{f_1^2}\right)$ is used to convert $I^s_{r,1}(i)$ in

meters to line-of-sight TEC $I^s_{r,1}(i)$ in TECu; $b_r = b_{r,2} - b_{r,1}$ and $b^s = b^s_{,2} - b^s_{,1}$ are the receiver and satellite IFBs; $\varepsilon_L(i)$ is the effect of un-modeled errors for CPIOs, which is around 100× smaller than $\varepsilon_P(i)$ for CIOs.

Once the CIOs and CPIOs are available, a leveling constant B_{rs} is then determined per continuous satellite arc (within which the set of CPIOs share a common ambiguity):

$$\begin{aligned} B_{rs} &= \sum_{i=1}^{M} \frac{1}{\sigma_i^2}\left(P^s_{r,1}(i) - L^s_{r,1}(i)\right) \Big/ \sum_{i=1}^{M}\left(1/\sigma_i^2\right) \\ &= \kappa\left[\left(b_r - b^s\right) - \left(N^s_{r,1} - N^s_{r,2}\right)\right] + \varepsilon_{P,\mathrm{arc}}(i), \end{aligned} \tag{3}$$

where σ_i is the standard deviation of $P^s_{r,1}(i)$; M is the number of epochs; $\varepsilon_{P,\mathrm{arc}}(i)$ is the weighted average of $\varepsilon_P(i)$ and $\varepsilon_L(i)$ within the continuous arc.

After adding B_{rs} in eq. (3) to $L^s_{r,1}(i)$ in eq. (2), the ambiguities are removed from the CPIOs and replaced by the b_r and b^s:

$$\begin{aligned} \tilde{L}^s_{r,1}(i) &= L^s_{r,1}(i) + B_{rs} \\ &= I^s_{r,1}(i) + \kappa\left(b_r - b^s\right) + \varepsilon_{P,\mathrm{arc}}(i), \end{aligned} \tag{4}$$

then the LIOs $\tilde{L}^s_{r,1}(i)$ follow.

From the derivations described above, two typical drawbacks underlying the carrier-to-code leveling process can be figured out: 1. By comparing the LIOs in eq. (4) with CIOs in eq. (2), the ε_P presented in CIOs may affect the LIOs, once their averaged quantities $\varepsilon_{P,\mathrm{arc}}(i)$ are not ideally zero ($\varepsilon_L(i)$ is negligible in eq. (4)); 2. A large amount of $\rho^s_r(i)$, which has been modeled (implicitly) as unknowns per epoch, per satellite, can be experienced along with increasing numbers of satellites and epochs. Besides, possible external information on $\rho^s_r(i)$ cannot be reasonably accounted for during the leveling process, since $\rho^s_r(i)$ is eliminated *a-priori* in observation domain.

1.2 Precise point positioning (PPP)

Since firstly proposed by Zumberge et al. [23] in 1997, the PPP has become a representative technique for high-precision positioning, time-transfer, and airborne survey [24–26]. In this subsection, the scope of applying PPP is further extended to ionosphere study, especially in the aspects of extracting ionospheric information.

The precise GPS orbits and clocks provided by IGS, with cm precision, are important prerequisite for PPP implementation [26]. Currently, the IGS products come in various flavors, from the Final, Rapid and Predicted to Ultra-Rapid [27]. They differ mainly by their varying latency and the extent of the tracking network used for their generation. In the following investigations, the IGS Final products with the highest precision (cm level) among others will be based on.

As a starting point, the $\rho^s_r(i)$ in eq. (1) can be further expanded as

$$\rho^s_r(i) = l^{\mathbf{s}}_{\mathbf{r}}(i) + \tau^{\mathbf{s}}_{\mathbf{r}}(i) + dt_r(i) - dt^s(i), \tag{5}$$

where $l^{\mathbf{s}}_{\mathbf{r}}(i)$ is the geometric range; $\tau^{\mathbf{s}}_{\mathbf{r}}(i)$ is the slant tropospheric delay; $dt_r(i)$ and $dt^s(i)$ are respectively the receiver and satellite clocks.

To simplify following derivations, the position of receiver is assumed known, then the deterministic value of $l^{\mathbf{s}}_{\mathbf{r}}(i)$ can be obtained by further accounting for the known position of satellite provided by IGS. Furthermore, the satellite clock from IGS can be given as

$$dt^s_I(i) = dt^s(i) + \underbrace{\alpha \cdot b^s_{,1} - \delta \cdot b^s_{,2}}_{b^s_{iff}}, \tag{6}$$

where $\delta = 1/\left(\mu_2 - 1\right)$ and $\alpha = \delta \cdot \mu_2$.

Based on known $l^{\mathbf{s}}_{\mathbf{r}}(i)$ and $dt^s_I(i)$, a re-formulated observation equations corresponding to eq. (1) can be given as (see Appendix for detailed derivations):

$$\begin{aligned} \overline{p}^s_{r,j}(i) &= \tau^s_r(i) + \overline{dt}_r(i) + \mu_j \cdot \overline{I}^s_{r,1}(i), \\ \overline{\phi}^s_{r,j}(i) &= \tau^s_r(i) + \overline{dt}_r(i) - \mu_j \cdot \overline{I}^s_{r,1}(i) + \overline{N}^s_{r,j}, \end{aligned} \tag{7}$$

where $\overline{p}^s_{r,j}(i)$ and $\overline{\phi}^s_{r,j}(i)$ denote the linearized code and carrier-phase, of which the $l^{\mathbf{s}}_{\mathbf{r}}(i)$, $dt^s_I(i)$ and any other system errors exceeding cm level have been a-priori corrected; $\overline{dt}_r(i)$, $\overline{I}^s_{r,1}(i)$ and $\overline{N}^s_{r,j}$ are the estimable receiver clock, ionospheric delays and carrier-phase ambiguities biased by the $b^s_{,j}$ and $b_{r,j}$; the un-modeled errors are omitted here for briefness.

The $\overline{I}^s_{r,1}(i)$ in eq. (7),

$$\overline{I}^s_{r,1}(i) = \frac{40.28}{f_1^2} \cdot \tilde{L}^s_{r,1}(i), \tag{8}$$

is PIOs, as eq. (7) used for extracting the ionospheric observables in this paper is in essence equivalent to the basic observation equations adopted by the PPP (see ref. [24]).

By incorporating all available observation equations like eq. (7), and converting the $\tau^s_r(i)$ to zenith tropospheric delays (ZTD) by a mapping function, estimable unknowns can be determined using weighed least square method by fully accounting for their respective temporal behaviors: the ambiguities are modeled as time constant parameters; ZTDs are modeled as piece-wise parameter, i.e. time-constant within certain time interval (usually 2 h); both the receiver

clock errors and PIOs are modeled as epoch-wise parameters, which means a new set of unknowns are introduced for each epoch.

Eq. (8) shows that the PIOs in units of meters have coincidently the same form as the LIOs in eq. (4) in units of TECu, i.e. both PPP and the leveling process can generate ionospheric observables with identical form. However, the parameterization of $\rho_r^s(i)$ constitutes the main discrepancy between both procedures: by fixing the available IGS orbit/clocks, the large amount of $\rho_r^s(i)$ in the leveling process can be reasonably reduced to minor ZTDs and receiver clocks in PPP. It is expected that the decreasing unknowns that have to be estimated from the same amount of data would cause much alleviating propagation of the model formal errors to the unknowns.

In the following numerical tests, the standard deviation of GPS observations $\sigma_i = \sigma_0 / \sin\left(E_r^s\right)$ is assumed to be satellite elevation angle E_r^s dependent, and the constant σ_0 is selected as 3 dm or 3 mm for code or carrier-phase. In addition, a minimal elevation cutoff of 5° is applied for extracting PIOs to guarantee the full separability of all estimable unknowns, whereas 15° is applied for code-to-carrier leveling process to avoid processing particularly noisy (code) observations. All extracted PIOs with elevation angles less than 15° are then excluded to facilitate fair comparison with their LIOs counterparts.

2 Analysis methods and results

The components constituting the extracting error underlying LIOs or PIOs can be divided into three classes [15, 16]:

$$\xi_e = \xi_r + \xi^s + \xi_r^s , \tag{9}$$

where ξ_e is the lump sum of extracting error; ξ_r refers to the multipath effects and observational noise components originating from the environment surrounding the receiver/antenna; ξ^s refers to satellite-dependent components that affect PIOs only, e.g. errors of interpolating IGS orbit/clock; ξ_r^s is the satellite-receiver ray path dependent components contributed by azimuth- and elevation-dependent uncalibrated receiver and satellite antenna phase center variations [28].

Of all three categories of extracting error components listed above, ξ_r is the most predominant whose multipath components can reach several TECu as reported in ref. [13]; if the sampling interval of the GPS observations is consistent with the IGS clocks, the component of ξ^s arising from interpolation of IGS clocks can be largely reduced (as in the case of following co-location experiment), and the remaining component of ξ^s contributed by interpolation of IGS orbit is always less than several cm [26], and therefore can be safely disregarded; the ξ_r^s is always at levels several mm, whose effects will hereafter be ignored. In this section, based on the respective co-location and sTEC estimation experiments, the reduced effects of extracting error on PIOs in comparison with LIOs will be verified.

2.1 Co-location experiment

The magnitude of ξ_r in eq. (9) can be assessed by performing an experiment based on comparison of ionospheric observables obtained from co-located receivers. Single difference of ionospheric observables from the same satellite tracked simultaneously by co-located receivers, *A* and *B*, yields to eq. (10a) for LIOs and eq. (10b) for PIOs.

$$\Delta I_{,I}^s = \tilde{L}_{A,I}^s - \tilde{L}_{B,I}^s = \underbrace{b_A - b_B}_{\Delta b} + \underbrace{\xi_{A,I} - \xi_{B,I}}_{\Delta\xi_I} , \tag{10a}$$

$$\Delta I_{,P}^s = \overline{I}_{r,A}^s - \overline{I}_{r,B}^s = \Delta b + \underbrace{\xi_{A,P} - \xi_{B,P}}_{\Delta\xi_P} , \tag{10b}$$

where Δ is the between-receiver single difference operator (the satellite IFBs, sTEC and ξ^s in eq. (9) are cancelled by the single difference computation), and sub-indexes *I* and *P* refer to the LIOs and PIOs.

According to eq. (10), if the extracting error whose component of ξ_r is absent, the $\Delta I_{,I}^s$ or $\Delta I_{,P}^s$ should be ideally a constant independent of observed satellite, Δb, defined as the difference of the IFBs of receivers. As the existence of ξ_r will cause the data belonging to different satellite arcs deviate from Δb by an arc-dependent quantity, the spread of $\Delta I_{,I}^s$ or $\Delta I_{,P}^s$ between each satellite arcs can be a good indicator to reveal the extent to which the effects of ξ_r have been removed.

Table 1 describes the relevant characteristics of the zero- and short-baselines used in the co-location experiment: the four-character station name, receiver and antenna type, the location of the receivers (in latitude/longitude), and the days of year (DOY) covered by the arbitrarily chosen observations. All the GPS observations at the standard 30-sec sampling rate plus the IGS orbit/clock involved in this study are downloaded from the IGS data center (ftp://cddis.gsfc.nasa.gov).

In addition, it is known that the observations from certain GPS satellite to both receivers that form a zero-baseline are identically affected by the multipath, which means the $\Delta I_{,I}^s$ or $\Delta I_{,P}^s$ in eq. (10) can be free from the influence of multipath in the zero-baseline case, and then the effects of observational noise components of ξ_r in eq. (9) can be individually analyzed.

Table 1 Description of short- and zero-baselines used in the co-location experiments

Station	Receiver type	Antenna type	Location	Observing sessions	Note
STR1	LEICA GRX1200GGPRO	ASH701945C_M NONE	149.0°E, 35.3°S	2010, days 001 – 003	Short baseline 0.26 m
STR2	TRIMBLE NETR5	TPSCR3_GGD CONE			
YAR2	ASHTECH UZ-12	AOAD/M_T JPLA	115.3°E , 29.0°S		18.26 m
YAR3	LEICA GRX1200GGPRO	LEIAR25 NONE			
ADE1	ASHTECH Z-XII3	ASH700936B_M SNOW	138.6°E, 34.7°S	2010, day 001 – 003	Zero baseline
ADE2					
BUE1			58.5°W, 34.6°S	2009, day 001 – 003	
BUE2					
WEL1			174.8°E, 41.3°S,		
WEL2					

Representative cases of zero- and short-baseline experimental results are depicted in Figures 1 and 2, where (a) and (b) in each figure manifest a maximum between-arc difference, whereas (c) and (d) show the cases with the minimal difference found in our investigation.

The effects of observational noise on LIOs, as inferred from the spread between single differences corresponding to different arcs in Figure 1(a) and (c), can reach respectively $\left(3/\sqrt{2}\right)/2 \approx 1.1$ TECu for the ADE1-ADE2 configuration and $\left(1.2/\sqrt{2}\right)/2 \approx 0.4$ TECu for the WEL1-WEL2 configuration, where the values 3 and 1.2 in the numerator of the fractions are the peak-to-peak values of the arc-to-arc spread in both panels; the $\sqrt{2}$ stems from the assumption that the error of a single-difference observation is roughly $\sqrt{2}\times$ greater than the error of un-difference ones; the denominator 2 indicates a 95% significance is used to evaluate the observational noise. Comparatively, the effects of observational noise on the PIOs, as derived from (b) and (d) by analogy, are respectively $\left(2.9/\sqrt{2}\right)/2 \approx 1.0$ and $\left(0.8/\sqrt{2}\right)/2 \approx 0.3$ TECu for the aforementioned two configurations. According to the rough estimate of the expected error in the LIOs (see ref. [13]), i.e. no greater than a fraction of TECu, the reduced extracting error effect arising from the observational noise on PIOs compared to LIOs is not statistically significant; in other words, both the carrier-to-code leveling and the proposed PPP procedures can

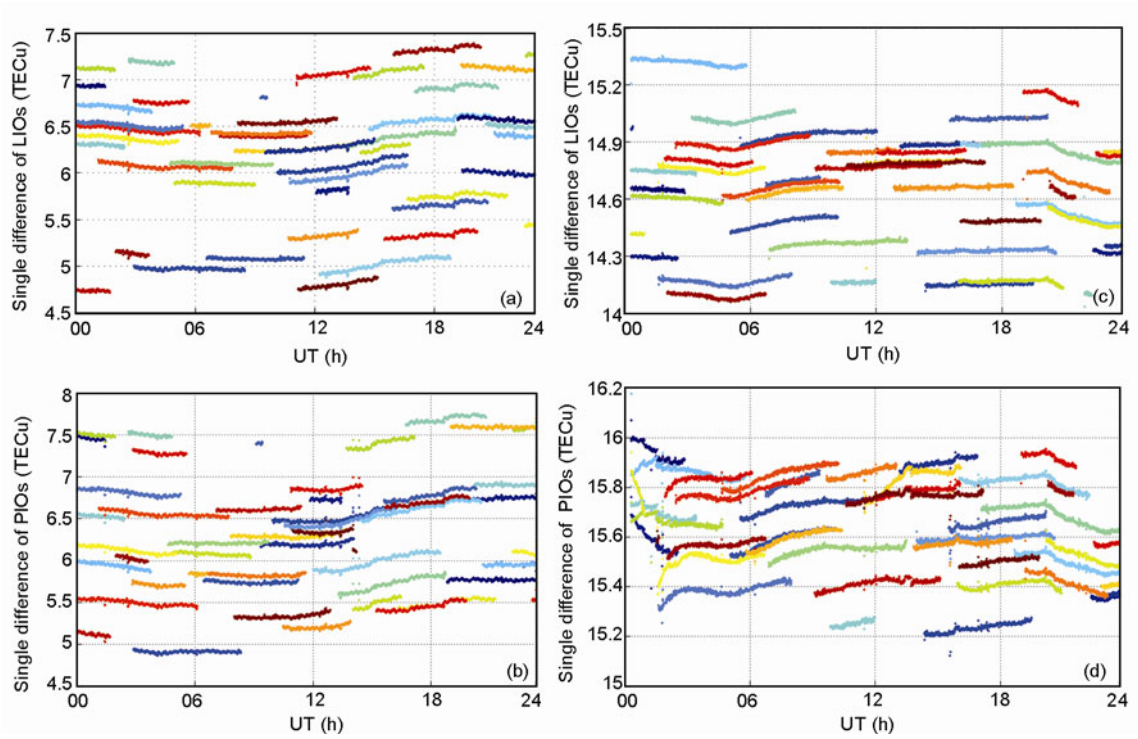

Figure 1 The between-receiver single difference of the LIOs and PIOs for representative zero-baselines (different colors correspond to different satellites). (a) and (b) ade1 and ade2, day 01/10; (c) and (d) wel1 and wel2, day 02/09.

effectively attenuate the influence of observational noise on the resulted ionospheric observables.

Whereas, from the short-baseline experimental results as shown in Figure 2, the significantly reduced extracting error effects on PIOs can be found: on day 01/10 for the STR1-STR2 configuration, the arc-to-arc spread can reach a peak-to-peak value of almost 5.5 and 1.5 TECu for LIOs and PIOs, which leads to an extracting errors of $\left(5.5/\sqrt{2}\right)/2 \approx 1.9$ and $\left(1.5/\sqrt{2}\right)/2 \approx 0.5$ TECu. On day 02/10 for the YAR2-YAR3 configuration, extracting error of $\left(4/\sqrt{2}\right)/2 \approx 1.4$ TECu can be found for LIOs and of $\left(1.1/\sqrt{2}\right)/2 \approx 0.4$ TECu for the PIOs.

The conclusions that can be drawn from this analysis are: (1) the proposed PPP method in this paper can result in a less multipath-affected ionospheric observables than the carrier-to-code leveling procedure; and (2) the amount of the extracting error underlying the PIOs as derived from the co-location experiments is approximately equal to the estimates of expected error that has been derived based on the assumption of absent multipath, which means the extent to which the multipath has been reduced with PPP is satisfactory.

2.2 sTEC estimation experiments

In this subsection, based on the widely used single-layer ionosphere model, the PIOs and the LIOs extracted from 26 successive days' observations from single GPS receiver are respectively used for retrieval of the satellite IFBs. As the design matrix of sTEC estimation with PIOs is identical to that with LIOs, the resulted PIO- and LIO-based satellite IFBs will be affected by identical model errors but different extracting errors, which means the well known daily reproducibility of GPS satellite IFBs [16, 29, 30] can be used to indirectly reflect the amount of extracting errors underlying PIOs or LIOs.

The experimental data came from two permanent IGS sites in equatorial and mid-latitude region (COCO, DAEJ) whose period spans from days 65 to 90 of 2001, i.e. closes to the Solar Maximum and includes Spring seasonal maximum of diurnal TEC, and some disturbed geomagnetic periods. During days 65–77, the geomagnetic activity was low to moderate ($K_p < 4$); in contrast, in the remaining days, the geomagnetic activity attained high and storm-level values in certain periods, with $6<K_p<9$ (http://ftp.gwdg.de/pub/geophys/kp-ap/tab/).

The reasons for the experimental data collection are two-fold: on the one hand, the reproducibility of retrieved satellite IFBs can be deemed as a limited case for studying ionosphere with GPS, as only the dataset from single GPS receiver at the extreme ionosphere condition is adopted together with the simplest ionosphere modeling approach; on the other hand, the between-receiver consistency of the PIO- or LIO-based satellite IFBs as derived from two remote IGS sites can also be used to examine the extent to

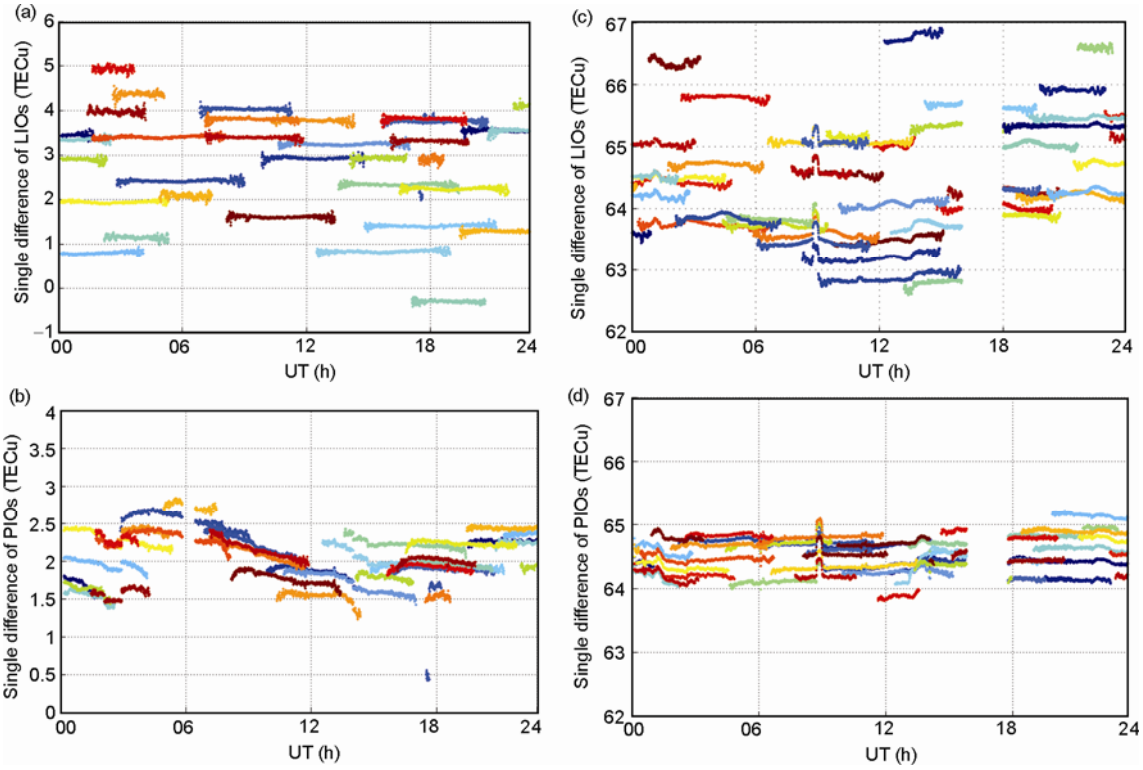

Figure 2 The between-receiver single difference of the LIOs and PIOs for representative short-baselines (different colors correspond to different satellites). (a) and (b): str1 and str2, day 01/10; (c) and (d): yar2 and yar3, day 02/10, data gaps are caused by missing observations from yar3.

which the receiver/antenna dependent extracting error has been reduced.

As only the IGS clock with a minimal sampling interval of 5 min is available during the period of the experiment, the extracted PIOs would inevitably be affected by the errors induced by the interpolation of IGS clocks. To avoid translation of severe clock interpolation error to the PIOs, during the PPP implementation, the problematic satellites with accuracy indicators (as specified in lines 8–12 of SP3 file) more than 6 are excluded.

The ionospheric model adopted in our experiment approximates the whole ionosphere with a spherical shell of infinitesimal thickness located at a given height, 350 km, above the Earth's surface. At the ionospheric penetration points (IPPs), the sTEC are mapped to the vTEC via the mapping function:

$$\frac{\text{vTEC}}{\text{sTEC}} \approx \cos z' = \sqrt{1-\left(\frac{R}{R+350}\right)^2 \cdot \cos^2(z)}, \qquad (11)$$

where R is the mean Earth's radius in units of km, z' and z are the GPS satellite's zenith angles at the IPP and the receiver's location.

The mathematical model selected to represent the temporal and spatial variability of vTEC reads

$$\text{vTEC} = a_{00}(t) + a_{10}(t)\cdot x + a_{01}(t)\cdot y, \qquad (12)$$

where t is the Universal Time and x and y are defined as $x = (\lambda_{\text{IPP}} - \lambda_{\text{R}})\cdot\cos(\phi_R)$ and $y = \mu_{\text{IPP}} - \mu_{\text{R}}$, of which the λ and ϕ are the geographic longitude and latitude, μ is the geomagnetic latitude, and the sub-indexes IPP and R refer to IPP and receiver. The coefficients $a_{ij}(t)$ are modeled as piece-wise unknowns whose updating interval is assumed to be 5 min for this investigation.

By arranging eqs. (4) (or eq. (8)), (11) and (12) together, the following observation equations for sTEC estimation can be obtained:

$$\begin{aligned} t_r^s(t) &= s\text{TEC}(t) + \kappa(b_r - b^s) \\ &= \sec z' \cdot \left[a_{00,k}(t) + a_{10,k}(t)\cdot x + a_{01,k}(t)\cdot y\right] + \kappa(b_r - b^s), \end{aligned} \qquad (13)$$

where $t_r^s(t)$ is the LIOs or PIOs in units of TECu; t is the epoch index within the 5-min time interval $[t_k, t_k + \Delta t]$.

Based on the LIOs or PIOs extracted from the GPS data from two IGS sites, the satellite IFBs are retrieved station-by-station on a daily basis. In addition, during the sTEC estimation with eq. (13), the condition of zero-mean satellite IFBs is imposed upon to avoid processing rank-defect observation equations.

Figure 3 reveals several representative satellite IFB values estimated from daily PIOs and LIOs. From the figure, the effects of the model error and the extracting error on the retrieved satellite IFBs can be respectively recognized: owing to the same model error effects, the PIO-based satellite IFB values manifest a similar inter-day variation behaviors with their counterparts as derived from LIOs; on the contrary, the reducing extracting error underlying PIOs compared with LIOs leads to a minor amplitude of the array of PIO-based daily satellite IFBs values. In addition, for several specific days, i.e. days 79, 80, etc., much pronounced satellite IFB variations can be found in Figure 3, which are caused by the much more disturbed ionosphere conditions in these days than the remaining days.

Furthermore, the averaged satellite IFB values within the days covered by the experiment plus their standard deviations (STDs) are listed in Figure 4, and the results are demonstrated via different manners.

Firstly, as derived from Figure 4(a), it is noticeable that the PIO-based satellite IFBs always experience more stable time-varying behavior than that resulted from the LIOs, as evidenced by their smaller STDs, i.e. ranging from 1 to 2.3 TECu compared with 1.3 to 4 TECu for LIO-based satellite IFBs. In addition, the first three maximal discrepancies of the mean value between the PIO- and LIO-based satellite IFBs as found in this experiment are 4.2, 3.4 and 2.1 TECu for PRN 6, 7 and 10, which are statistically significant by taking their STDs into consideration. For the satellite IFBs results as derived from DAEJ in Figure 4(b), the assertion still holds of more stable PIO-based satellite IFBs as concluded from Figure 4(a). In this case, the STDs of PIO-based satellite IFBs range from 0.3 to 1.1 TECu, while 0.7 to 2.2 for the LIO-based satellite IFBs; besides, the first three maximal discrepancies of the mean value between the PIO- and LIO-based satellite IFBs can reach 2.9, 1.5 and 1.1 TECu for PRN 13, 8 and 6.

Secondly, from Figure 4(c) and (d) (noticing their different vertical axis scales), the between-receiver consistencies of PIO- and LIO-based satellite IFBs can be respectively recognized: the differences of PIO-based satellite IFBs respectively based on the GPS observations from COCO and DAEJ range from 0.2 to 1 TECu; as for the case of LIOs, such differences range on average from 1–2 TECu for most satellites, but can exceed more than 3–4 TECu for several typical satellites (i.e. PRN 2 and 13). In addition, the improved satellite IFB results in terms of smaller STDs for DAEJ in contrast to COCO can be attributed to their different geographical locations: the COCO is much closer to the geomagnetic equator than the DAEJ, leading to more disturbed ionosphere conditions in COCO, and further pronounced intra-day behavior of resulted satellite IFBs.

In summary, the PIO-based satellite IFB values compare favorably in terms of inter-day reproducibility and between-receiver consistency with their counterparts as estimated from LIOs, and the only reason for this phenomenon can be attributed to the minor extracting error as experienced by the PIOs.

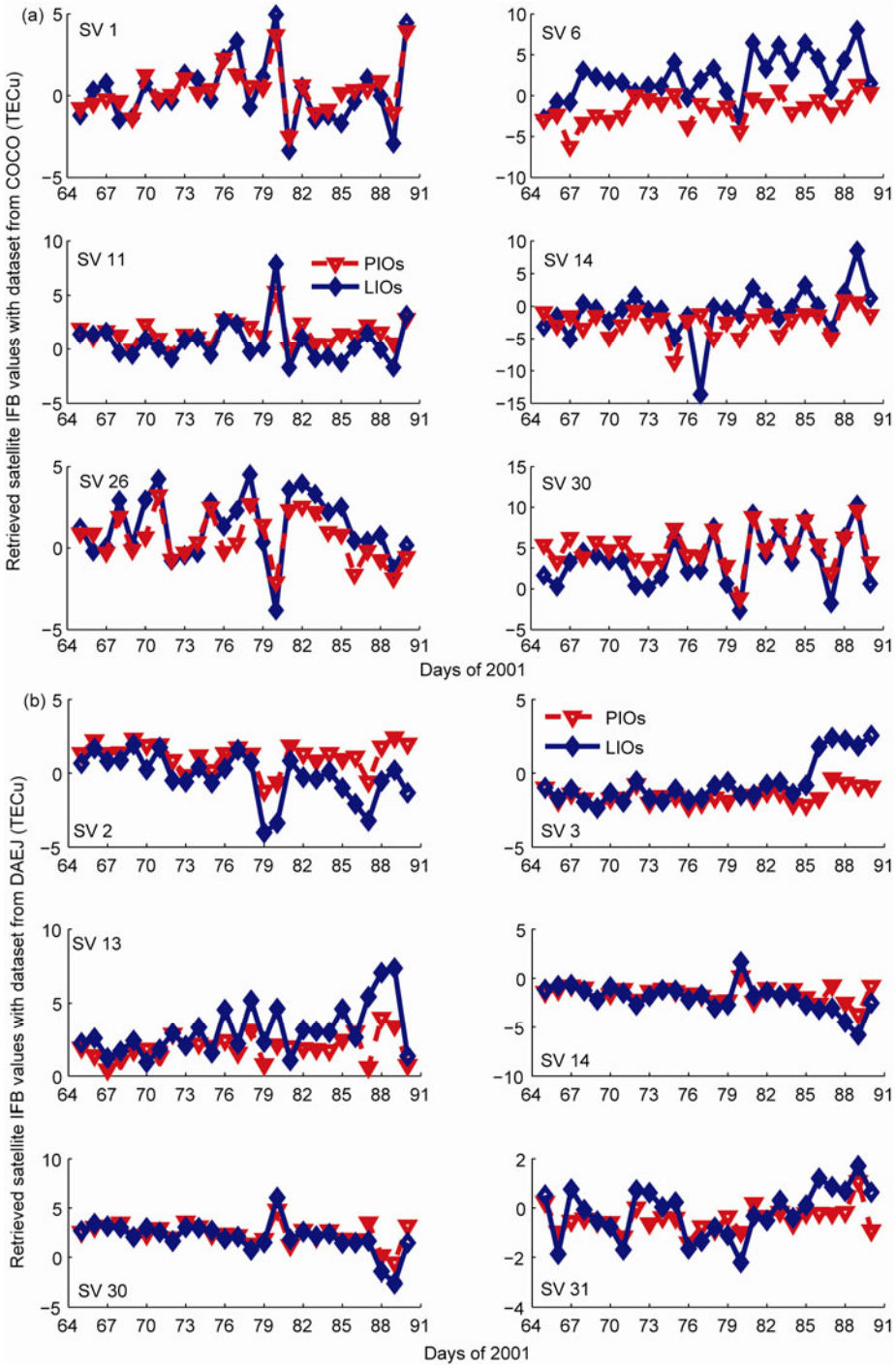

Figure 3 Daily satellite IFB values retrieved from PIOs and LIOs based on GPS datasets from COCO (a) and DAEJ (b) representative cases.

3 Discussion and summary

A new approach for extraction of the ionospheric observables with PPP is presented in this paper, and the resulted PIOs have coincidently the same forms as the LIOs that have been widely used for GPS-based ionospheric studies. From our derivation, it is found that the difference between the generation process of the PIOs and the LIOs lies in reducing the satellite arc-dependent ambiguities from the CPIOs: the former based on a geodetic data processing strategy whereas the latter mainly based on carrier- to-code leveling procedure.

The extracting errors underlying PIOs and LIOs are compared based on respectively the co-location and the sTEC estimation experiments: the former experiment can directly reflect the possible extracting error effects by in-

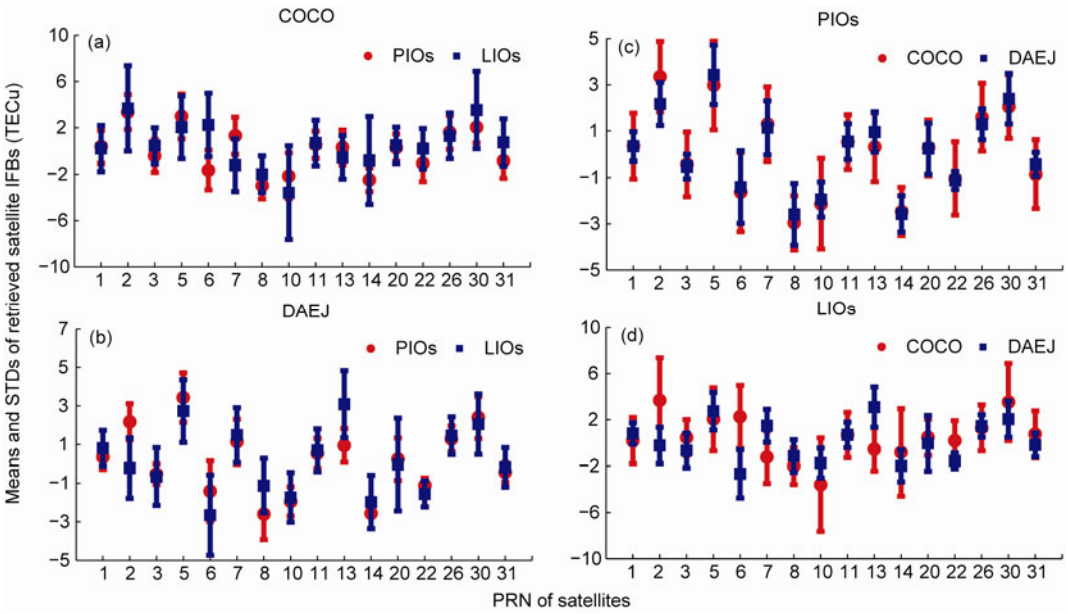

Figure 4 The means and standard deviations (STDs) of daily retrieved satellite IFB values. (a) and (b) denote station-wise results corresponding to IGS sites COCO and DAEJ based on respective PIOs and LIOs; comparatively, (c) and (d) depict the same results but sorted according to types of ionospheric observables (i.e. LIOs or PIOs) from different sites.

vestigating the spread of the single-differenced ionospheric observable corresponding to different satellite arcs, and the latter experiment can be used to reveal the effects of combined model and extracting errors on the retrieved satellite IFBs; the well-known temporal stability of satellite IFBs are used in this experiment to assess the effects of extracting errors.

The adequate reduction of the receiver/antenna dependent extracting error with PPP is validated by the above mentioned two experiments from the following aspects: (1) The amount of the extracting error underlying the PIOs as derived from the co-location experiment is ideally equal to the estimates of expected error that has been derived based on the assumption of absent multipath; (2) the reproducibility of PIO-based satellite IFBs can reach no more than 2.5 TECu based on the GPS observations from a near geomagnetic equator IGS site during extreme ionosphere conditions, whereas for LIO-based satellite IFBs, the result can be as large as 4 TECu; and (3) the PIO-based satellite IFBs retrieved from two remote IGS site manifest a consistency of no more than 1 TECu, but for LIO-based satellite IFBs, such values can be reach even to 3–4 TECu, which can adequately explain the unacceptable reduction of receiver/antenna dependent extracting error with carrier-to-code leveling process.

It should be noted that generation of PIOs is inevitably restricted by the availability of the IGS orbit/clock, and the interpolation of these products can lead to possible additional extracting errors in PIOs. Fortunately, since Dec. 2006, the IGS clock with a minimal sampling interval of 30 sec can be freely downloadable via the internet [27], which can meet the requirements of most GPS-based ionospheric studies. At the same time, the improving data processing strategies at each IGS analysis center can result in more and more accurate IGS products [26, 31].

Besides, as the PIOs are derived from a geodetic data processing procedure, regional ionosphere modeling based on PIOs would provide single-frequency navigation users with more consistent TEC corrections than based on LIOs, especially for equatorial or aurora regions with extreme ionosphere conditions [32]. In addition, possibly more realistic local features would be disclosed when mapping the ionosphere is based on the PIOs instead of LIOs, thus supplying a much more convincible reference for spatial science studies.

Appendix

The $b_{r,j}-b^s_{,j}$ in eq. (1) can be equivalently represented as

$$b_{r,j}-b^s_{,j}=b_{r,if}-b^s_{,if}+\beta_j\cdot\left(b_r-b^s\right), \tag{A1}$$

where $b_{r,if}=\alpha\cdot b_{r,1}-\delta\cdot b_{r,2}$ and $\beta_j=\mu_j\cdot\delta$; the detailed form of $b^s_{,if}$ is listed in eq. (6).

After corrected by the $l^s_{\mathbf{r}}(i)$ and $dt^s_I(i)$, the code equations for PPP can be formulated as (omitting the unmodeled errors):

$$\overline{p}^s_{r,j}(i)=\rho^s_r(i)+\mu_j\cdot I^s_{r,1}(i)-b^s_{,j}+b_{r,j}+b^s_{,if}, \tag{A2}$$

where $b^s_{,if}$ originates from $dt^s_I(i)$; by accounting for eqs.

(A1) and (5), eq. (A2) can be re-formulated as:

$$\overline{p}_{r,j}^{s}(i)=\tau_{\mathbf{r}}^{\mathbf{s}}(i)+\underbrace{\left(dt_r(i)+b_{r,if}\right)}_{d\overline{t}_r(i)}+\mu_j\cdot\underbrace{\left[I_{r,1}^{s}(i)+\delta\cdot\left(b_r-b^{s}\right)\right]}_{\overline{I}_{r,1}^{s}(i)}. \quad \text{(A3)}$$

By identical parameterization of $d\overline{t}_r(i)$ and $\overline{I}_{r,1}^{s}(i)$ as in code (eq. (A3)), the carrier-phase equations can be given as

$$\begin{aligned}\overline{\phi}_{r,j}^{s}(i)&=\tau_r^{s}(i)+d\overline{t}(i)-\mu_j\cdot\overline{I}_{r,1}^{s}(i)\\&\quad+\underbrace{N_{r,j}^{s}-\left(b_{r,if}-b_{,if}^{s}\right)+\beta_j\cdot\left(b_r-b^{s}\right)}_{\overline{N}_{r,j}^{s}}\cdot\end{aligned} \quad \text{(A4)}$$

Apparently from eq. (A4), due to the opposite sign of ionospheric group and phase delays, the estimable ambiguities $\overline{N}_{r,j}^{s}$ are biased by the combination of satellite and receiver code biases, whose concrete forms are listed above the curly bracket. After the procedures listed above, the final PPP observation equations as in eq. (7) are derived.

This work was supported by National Basic Research Program of China (Grant No. 2012CB82560X) and National Natural Science Foundation of China (Grant Nos. 41174015 and 41074013).

1 Yang Y X, Zeng A M. Adaptive filtering for deformation parameter estimation in consideration of geometrical measurements and geophysical models. Sci China Ser D-Earth Sci, 2009, 52: 1216-1222
2 Yang Y X, Zeng A M, Wu F M. Horizontal crustal movement in China fitted by adaptive collocation with embedded Euler vector. Sci China Earth Sci, 2011, 54: 1822–1829
3 Feng Y M, Li B F. Wide area real time kinematic decimetre positioning with multiple carrier GNSS signals. Sci China Earth Sci, 2010, 53: 731–740
4 Yang Y X, Li J L, Xu J Y, et al. Contribution of the Compass satellite navigation system to global PNT users. Chin Sci Bull, 2011, 56: 2813–2819
5 Hernández-Pajares M, Juan J M, Sanz J. New approaches in global ionospheric determination using ground GPS data. J Atmos Solar Terr Phys, 1999, 61: 1237–1247
6 Mannucci A J, Wilson B D, Yuan D N, et al. A global mapping technique for GPS derived ionospheric total electron content measurements. Radio Sci, 1998, 33: 565–582
7 Brunini C, Azpilicueta F. Accuracy assessment of the GPS-based slant total electron content. J Geod, 2009, 83: 773–785
8 Brunini C, Azpilicueta F. GPS slant total electron content accuracy using the single layer model under different geomagnetic regions and ionospheric conditions. J Geod, 2010, 84: 293–304
9 Komjathy A, Sparks L, Wilson B D, et al. Automated daily processing of more than 1000 ground-based GPS receivers for studying intense ionospheric storms, Radio Sci, 2005, 40: RS6006
10 Wilson B D, Mannucci A J. Extracting ionospheric measurements from GPS in the presence of Anti-Spoofing. Proceedings of ION GPS, Salt Lake City, Utah, USA. 1994. 1599–1608
11 Burrell A G, Bonito N A, Carrano C S. Total electron content processing from GPS observations to facilitate ionospheric modeling. GPS Solut, 2006, 13: 83–95
12 Rideout W, Coster A. Automated GPS processing for global total electron content data. GPS Solut, 2006, 10: 219–228
13 Ciraolo L, Azpilicueta F, Brunini C, et al. Calibration errors on experimental slant total electron content determined with GPS. J Geod, 2007, 81: 111–120
14 Yuan Y B, Huo X L, Ou J K. Models and methods for precise determination of ionospheric delay using GPS. Prog Nat Sci, 2007, 17: 187–196
15 Bishop G J, Klobuchar J A. Multipath effects on the determination of absolute ionospheric time delay from GPS signals. Radio Sci, 1985, 20: 388–396
16 Coco D S, Coker C, Dahlke S R, et al. Variability of GPS satellite differential group delays biases. IEEE Trans Aerosp Electron Syst, 1991 27: 931–938
17 Manucci A J, Iijima B A, Lindqwister U J, et al. GPS and ionosphere: URSI reviews of Radio Science, Jet Propulsion Laboratory, Pasadena, 1999
18 Hernández-Pajares M, Juan J M, Sanz J, et al. Improvig the real-time ionopsheric determination from GPS sites at very long distances over the equator. J Geophys Res, 2002, doi: 10.1029/2001JA009203
19 Schaer S, Beutler G, Mervart L, et al. Global and regional ionosphere models using the GPS double difference phase observable. In: Gendt G, Dick G, eds. Proceedings of the IGS Workshop on Special Topics on New Directions, Potsdam, 1995. 77–92
20 Wanninger L. Enhancing differential GPS using regional ionospheric error models. J Geod, 1995, 69: 283–291
21 Wilson B D, Mannucci A J. Instrumental Biases in Ionospheric Measurements derived from GPS data. Proceedings of ION GPS, Salt Lake City, Utah, USA, 1993
22 Mitchell C N, Spencer P S J. A three-dimensional time-dependent algorithm for ionospheric imaging using GPS. Ann Geophys, 2003, 46: 687–696
23 Zumberge J F, Heflin M B, Jefferson D C, et al. Precise point positioning for the efficient and robust analysis of GPS data from large networks. J Geophys Res, 1997, 102: 5005–5017
24 Liu J N, Ye S R. GPS Precise point positioning using undifferenced phase observation (in Chinese). Geomat Inf Sci Wuhan Univ, 2002, 27: 234-240
25 Zhang X H, Liu J N, Forsberg R. Application of precise point positioning in airborne survey (in Chinese). Geomat Inf Sci Wuhan Univ, 2006, 31: 19–22, 46
26 Kouba J, Heroux P. GPS precise point positioning using IGS orbit products. GPS Solut, 2001, 5: 12–28
27 Dow J, Neilan R, Rizos C. The international GNSS service in a changing landscape of global navigation satellite systems. J Geod, 2009, 83: 191–198
28 Schmid R, Steigenberger P, Gendt G, et al. Generation of a consistent absolute phase-center correction model for GPS receiver and satellite antennas. J Geod, 2007, 81: 781–798
29 Sardon E, Zarraoa N. Estimation of total electron-content using GPS data: How stable are the differential satellite and receiver instrumental biases? Radio Sci, 1997, 32: 1899–1910
30 Gaposchkin E M, Coster A J. GPS L1–L2 bias determination. Lincoln Laboratory Technical Report 971 (MIT), Massachusetts, 1993
31 Zhang B C, Ou J K, Yuan Y B, et al. Yaw attitude of eclipsing GPS satellites and its impact on solutions from precise point positioning. Chin Sci Bull, 2010, 55: 3687−3693
32 Camargo P O, Monico J F G, Ferreira L D D. Application of ionospheric corrections in the equatorial region for L1 GPS users. Earth Planets Space, 2000, 52: 1083–1089